http://dx.doi.org/10.5012/bkcs.2014.35.5.1379

Comparison of the Kinetic Behaviors of Fe_2O_3 Spherical Submicron Clusters and Fe_2O_3 Fine Powder Catalysts for CO Oxidation

Seung-Gyun Yoo, Jin-Hoon Kim, Un-Ho Kim,[†] Jin-Seung Jung,[†,*] and Sung-Han Lee[*]

Department of Chemistry, Yonsei University, Wonju 220-710, Korea. [*]E-mail: shl2238@yonsei.ac.kr
[†]Department of Chemistry, Gangneung-Wonju National University, Gangneung 210-702, Korea. [*]E-mail: jjscm@gwnu.ac.kr
Received October 26, 2013, Accepted January 16, 2014

α-Fe_2O_3 spherical particles having an average diameter of *ca.* 420 nm and α-Fe_2O_3 fine particles (< 10 μm particle size) were prepared to examine as catalysts for CO oxidation. Kinetic studies on the catalytic reactions were performed in a flow reactor using an on-line gas chromatography system operated at 1 atm. The apparent activation energies and the partial orders with respect to CO and O_2 were determined from the rates of CO disappearance in the reaction stage showing a constant catalytic activity. In the temperature range of 150-275 °C, the apparent activation energies were calculated to be 13.7 kcal/mol on the α-Fe_2O_3 spherical submicron clusters and 15.0 kcal/mol on the α-Fe_2O_3 fine powder. The Pco and Po_2 dependencies of rate were investigated at various partial pressures of CO and O_2 at 250 °C. Zero-order kinetics were observed for O_2 on both the catalysts, but the reaction order for CO was observed as first-order on the α-Fe_2O_3 fine powder and 0.75-order on the α-Fe_2O_3 spherical submicron clusters. The catalytic processes including the inhibition process by CO_2 on the α-Fe_2O_3 spherical submicron powder are discussed according to the kinetic results. The catalysts were characterized using XRD (X-ray powder diffraction), FE-SEM (field emission-scanning electron microscopy), HR-TEM (high resolution-transmission electron microscopy), and N_2 sorption measurements.

Key Words : Iron oxide clusters, Catalytic oxidation of CO, Kinetics, Inhibition process by CO_2

Introduction

Catalytic oxidation of CO is one of the most important reactions in environmental catalysis. Transition metal oxides like MnO_2, Fe_2O_3, NiO, and CuO were found to be active catalysts for CO oxidation and the transition metal oxide-supported noble metal catalysts were proved to be highly active for the low-temperature CO oxidation.[1-4] Fe_2O_3 is considered as one of alternatives to the noble metal catalysts for CO oxidation because of its efficiency and low cost.[1,4] Fe_2O_3 is particularly attractive owing to its dual functions for CO oxidation as a catalyst of CO in the presence of gaseous oxygen and as a direct oxidant of CO in the absence of gaseous oxygen.[5]

In general, catalytic properties of materials largely depend on their particle size and porosity. During the last two decades, nanostructured metal oxides have been extensively studied as new materials for catalyst or catalyst support because they have high surface area. Li *et al.*[5] have demonstrated that Fe_2O_3 nanopowder catalyst is much more effective for CO oxidation than the non-nano powder catalyst. In recent years, cluster materials have been of great interest in both basic science and applied science because their physical and chemical properties are remarkably different from those of the corresponding non-cluster materials.[6-10] Some investigators have reported the unique properties of metal oxide clusters as catalyst.[11,12] Iron oxide clusters are especially attractive because they can be synthesized in the form of submicron particles with well-controlled size and shape.[13] Iron oxide submicron particles are formed by a self-assembly process of nanoparticles, in which iron oxide nanocrystals interweave together to form the submicron particles having internal pores. At present, little is known about the catalytic behaviors of iron oxide spherical submicron clusters.

This paper reports the first study of the catalytic properties of α-Fe_2O_3 spherical submicron clusters. In this work, the catalytic oxidation of carbon monoxide was studied as a test reaction to investigate the potential application of Fe_2O_3 submicron clusters as catalyst. We prepared α-Fe_2O_3 spherical submicron particles having an average diameter *ca.* 420 nm using an one-step solvothermal method. Kinetic measurements for the catalytic reaction were performed in a flow reactor system. The apparent activation energy and reaction orders with respect to both CO and O_2 were determined from the rates of CO disappearance. The catalytic behaviors of the α-Fe_2O_3 submicron powder for CO oxidation were compared with those of α-Fe_2O_3 fine powder as a reference. We observed the inhibition effect by CO_2 on the reaction rate in the CO oxidation over α-Fe_2O_3 spherical submicron particles. The present kinetic results were compared with those reported previously and were utilized to deduce the reaction mechanism.

Experimental

α-Fe_2O_3 submicron particles were obtained by oxidizing magnetite submicron particles. Magnetite submicron particles were synthesized from $FeCl_3 \cdot 6H_2O$ (97%, Aldrich-Sigma), sodium acetate trihydrate (NaAc) (99+%, Aldrich-Sigma), and ethylene glycol (EG) (≥ 99%, Aldrich-Sigma) using the

solvothermal reduction method reported by Deng *et al.*.[13] $FeCl_3 \cdot 6H_2O$ (1.08 g) and NaAc (3.0 g) were dissolved in EG (40 mL) to form a clear solution, and then this mixture was vigorous stirred for 30 min. As-formed viscous slurry was transferred into a teflon-lined stainless-steel autoclave of 80 mL capacity. The autoclave was maintained at 200 °C for 10 h and cooled to room temperature to obtain precipitates. The resulting precipitates were washed with distilled water and absolute alcohol several times, dried at 60 °C for 6 h, and black powder was obtained. The black powder was calcined at 600 °C in a flow of O_2(g), cooled to room temperature, and red powder was obtained. α-Fe_2O_3 fine powder as a reference was prepared from $FeCl_3 \cdot 6H_2O$ and NH_4OH solution.[14] $FeCl_3 \cdot 6H_2O$ was dissolved in deionized water, the iron chloride solution was added into the 0.38 M NH_4OH solution with constant stirring, and precipitates were immediately produced. The precipitates were washed with deionized water until the wash liquor was free of chlorides, dried at 50 °C, calcined at 600 °C in air and red powder was obtained. The red powder was identified as rhombohedral hematite (α-Fe_2O_3) by XRD analysis. The α-Fe_2O_3 powder was passed through a standard sieve to gather the particles having particle size less than 10 μm. The obtained samples were characterized by XRD (X-ray powder diffraction), FE-SEM (field emission-scanning electron microscopy), HR-TEM (high resolution-transmission electron microscopy), and N_2 sorption measurements. To identify the phases and crystalline structures, XRD patterns of the samples were taken on a Bruker D2 Phaser diffractometer and the XRD data were compared with those in the JCPDS File. FE-SEM and HR-TEM images were obtained using a Hitachi SU70 and a JEOL JEM-2100, respectively. N_2 sorption measurements were performed using a Micromeritics automatic gas adsorption system (ASAP 2010). The specific surface areas were measured by the BET method and the pore size distribution was obtained from the adsorption branch of the N_2 adsorption-desorption isotherm by the BJH method.

Kinetic measurements were carried out in a fixed-bed type continuous flow reactor operated at atmospheric pressure. The microreactor was quartz tubing with a 0.8-cm-i.d. and 3-cm-long tube sealed to 0.4-cm-i.d. tubes on two ends. The catalyst (150 mg) was well dispersed on porous fused-silica bed placed in the middle of the reactor. A K-type thermocouple was contacted with the outside wall of the reactor next to the catalyst bed to control the reaction temperature. The catalyst was pretreated at 600 °C in a flow of O_2 for 1 h after loading into the reactor and cooled to room temperature in a flow of He. The reaction mixture containing CO, O_2, and He as a diluent gas was then introduced into the microreactor at a desired temperature. The purity of the gases was better than 99.99% and each gas was passed through a bed of molecular sieve to remove water before introducing it into the reactor. The flow rate of each gas was controlled by electronic mass flow controller. The total flow rate of reaction mixture (CO/O_2/He) was 70 cm^3/min. The gas stream was analyzed by using an on-line gas chromatography system equipped with a thermal conductivity detector (HP5890+) and gas compositions were determined using an external standard gas mixture. The conversions of CO and O_2 in the catalytic reaction were measured in the reaction stage showing a constant catalytic activity. The CO conversion data used for kinetic calculations were limited to the values less than 10%. The reaction rates were calculated based on the conversions of CO: rate = Cco × Vco/22400 × W, where Cco is the CO conversion, Vco the volume flow rate of CO (cm^3/min), and W the catalyst weight (g).

Results

Figure 1(a) shows the XRD pattern of the magnetite powder obtained using the solvothermal reduction method, indicating that the diffraction pattern corresponds to the face-centered cubic magnetite (Fe_3O_4) structure (JCPDS Card No. 00-039-1346). Figure 1(b) shows the XRD pattern of the red powder obtained after the calcination of the magnetite powder at 600 °C, indicating that the red powder corresponds to the hematite (α-Fe_2O_3) with rhombohedral structure (JCPDS Card No. 01-089- 0598).

The XRD results indicate that the magnetite phase was completely transformed into the hematite phase during the calcination process. To determine the size and particle morphology of the submicron particles, FE-SEM and HR-TEM analyses were performed. Figure 2(a) exhibits the FE-SEM image of the magnetite submicron particles with the controlled size. All the particles show a spherical morphology with a rough surface and the average diameter of the

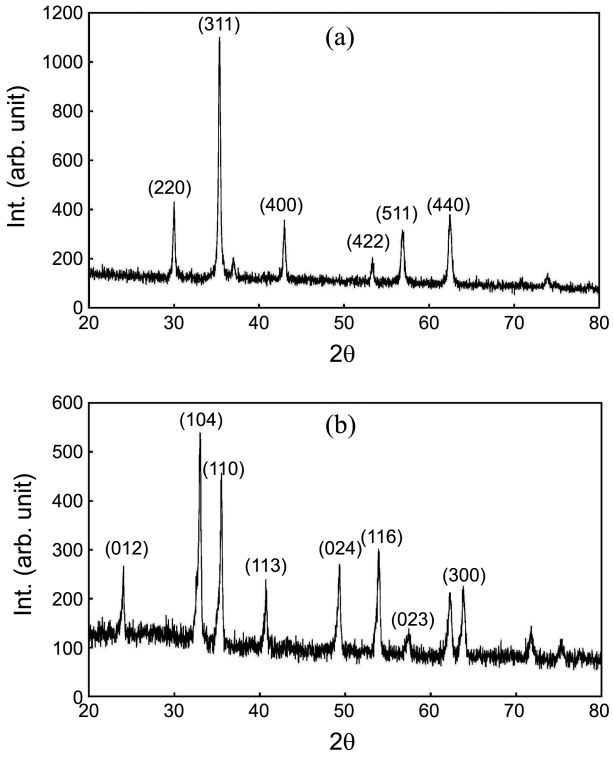

Figure 1. XRD patterns of (a) the magnetite powder obtained using the solvothermal method and (b) the calcined magnetite powder.

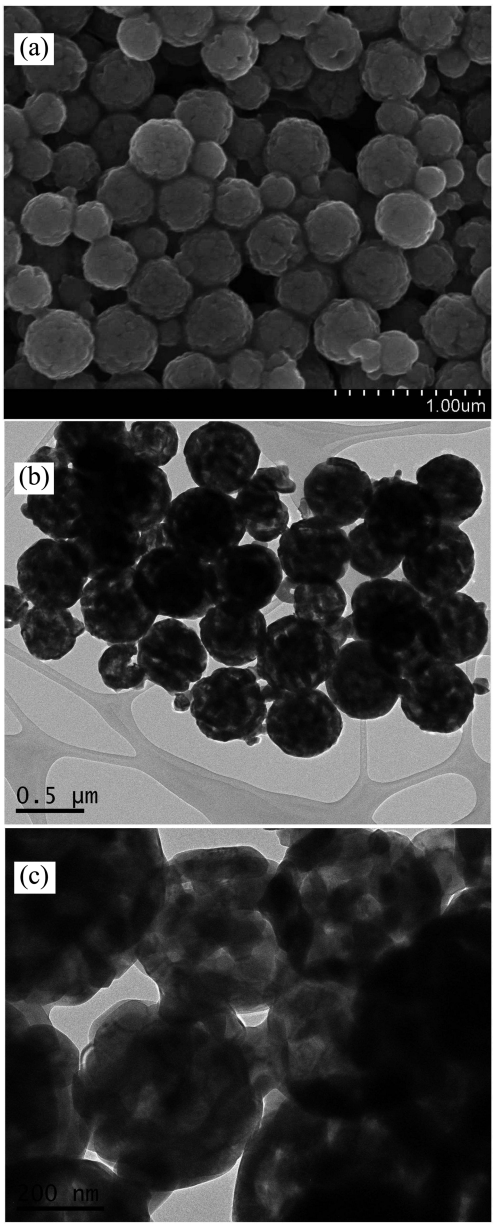

Figure 2. (a) SEM image of the magnetite powder prepared using the solvothermal method, (b) TEM image of the calcined magnetite powder, and (c) TEM image of the calcined magnetite powder at a higher magnification.

particles is *ca.* 420 nm. Figure 2(b) shows the HR-TEM image of the α-Fe_2O_3 submicron particles. The electron microscopy results indicated that there was no significant change in the spherical morphology between the uncalcined and calcined magnetite submicron clusters. As observed in Figure 1, the XRD peaks show a peak broadening, implicating that the component crystallites are of nanoscale character. Using the Scherrer equation, $d = 0.9\lambda/B\cos\theta$, the average size of the component crystallites of the α-Fe_2O_3 spherical submicron clusters was calculated to be *ca.* 24.9 nm. Figure 2(c) displays the HR-TEM image of the α-Fe_2O_3 spherical submicron clusters at a higher magnification, showing internal pores of the submicron particles. The BET

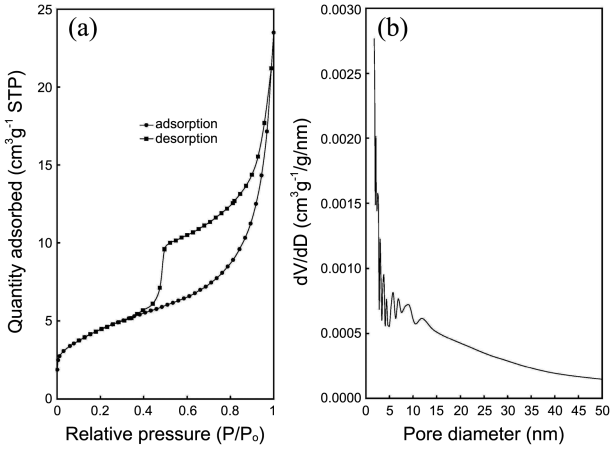

Figure 3. (a) N_2 adsorption-desorption isotherm and (b) the corresponding pore size distribution of the α-Fe_2O_3 spherical submicron clusters.

surface areas were determined to be 84.9 m^2/g for the α-Fe_2O_3 spherical submicron particles and 7.0 m^2/g for the α-Fe_2O_3 fine powder, which implies that the α-Fe_2O_3 spherical submicron particles may be porous. To confirm the porous structure of the α-Fe_2O_3 spherical submicron particles, a N_2 adsorption-desorption measurement was performed to characterize the internal pore structure. Figure 3(a) depicts the N_2 adsorption-desorption isotherm. Based on the shape of the curve, the isotherm can be classified as type IV which is characteristic of mesoporous materials. This hysteresis loop belongs to the H3 type which is typically observed for the wide capillaries having narrow openings and the mesoporous structures formed by nanoparticle assembly.[15,16] Figure 3(b) depicts the pore size distribution which was determined by the BJH method from the adsorption branch of the isotherm. The pores size distribution curve shows several mesopore peaks in the range of 3-20 nm, indicating the heterogeneity of the pores, which is considered to be mainly caused by interspace between the component nanoparticles.

The catalytic activities of the α-Fe_2O_3 spherical submicron clusters and the α-Fe_2O_3 fine powder for CO oxidation were measured in a flow of reaction mixture containing CO/O_2/

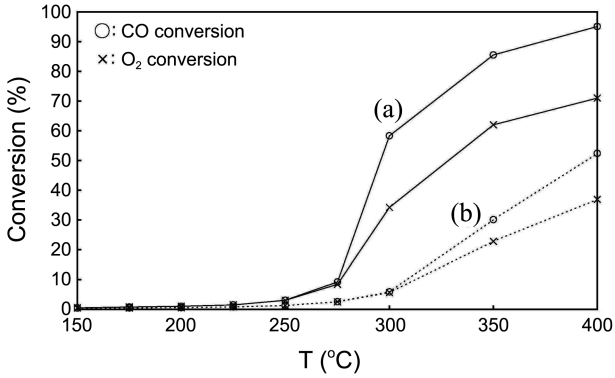

Figure 4. Variations of CO and O_2 conversions with temperature for the CO oxidations on (a) the α-Fe_2O_3 spherical submicron powder and (b) the α-Fe_2O_3 fine powder. Catalyst weight: 150 mg.

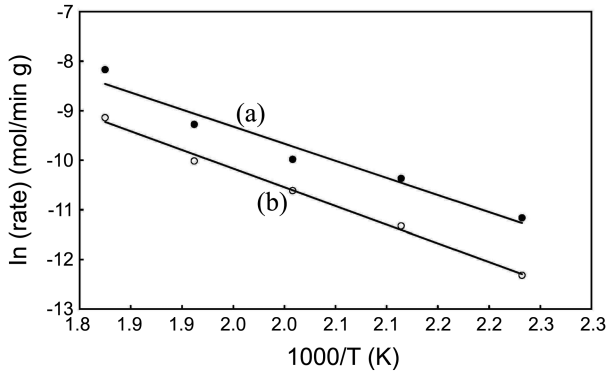

Figure 5. Arrhenius plots for the CO oxidations catalyzed by (a) the α-Fe_2O_3 spherical submicron powder and (b) the α-Fe_2O_3 fine powder. Catalyst weight: 150 mg.

He(10/5/55 cm^3/min) in the temperature range of 150-400 °C. In these experiments, the activities of catalysts were constant after 1 h time-on-stream. Both the CO and O_2 conversions were typically measured after 2 h time-on-stream. Figure 4 shows variations of the CO and O_2 conversions with temperature on both the catalysts in the range of 150-400 °C under the flow of reaction mixture containing CO/O_2/He (10/5/55 cm^3/min). The CO conversion on the α-Fe_2O_3 submicron powder was much higher than that on the α-Fe_2O_3 fine powder above 275 °C. At 400 °C, the CO conversions were measured as 95% on the α-Fe_2O_3 spherical submicron clusters and 52% on the α-Fe_2O_3 fine powder.

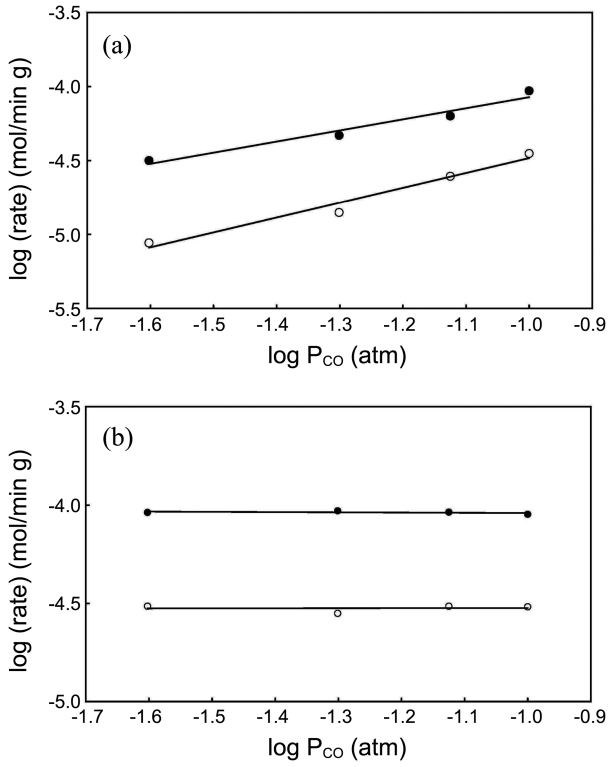

Figure 6. (A) *P*co and (B) Po_2 dependencies of rates for the CO oxidations catalyzed by (●) the α-Fe_2O_3 spherical submicron powder and (○) the α-Fe_2O_3 fine powder at 250 °C. Catalyst weight: 150 mg.

The apparent activation energies were determined from the rates which were measured in a flow of the reaction mixture containing CO/O_2/He (=10/5/55 cm^3/min). In the temperature range of 150-275 °C, the rates were plotted as a function of reciprocal temperature according to the Arrhenius-type equation, rate $\propto$ Aexp($-E_a$/RT), as shown in Figure 5. The apparent activation energies obtained from the Arrhenius plots were 13.7 kcal/mol on the α-Fe_2O_3 spherical submicron clusters and 15.0 kcal/mol on the α-Fe_2O_3 fine powder. The present values are higher than those (< 10 kcal/mol) for the CO oxidation on the Fe_2O_3-supported noble metal catalysts,[1] but they are close to 14.5 kcal/mol on the α-Fe_2O_3 nanoparticle catalyst.[5] To determine the partial orders with respect to CO and O_2, the rates were measured at various partial pressures of CO and O_2 at 250 °C. The rates were plotted as a function of partial pressures of CO and O_2 according to the equation, rate = $kPo_2^{\alpha}Pco^{\beta}$. Figure 6 shows the Pco and Po_2 dependencies of rate in the catalytic reaction. The reaction orders for CO and O_2 were determined from the slopes of linear curves. Zero-order kinetics were observed for O_2 on both the catalysts, but the reaction orders for CO were observed to be first-order on the α-Fe_2O_3 fine powder catalyst and 0.75-order on the α-Fe_2O_3 spherical submicron clusters.

Discussion

It is a generally known fact that the CO oxidation over Fe_2O_3 catalyst occurs in two successive stages, the reduction of the catalyst surface by CO and the oxidation of the reduced surface by O_2. As shown in Figure 4, the CO conversion is nearly equal to the O_2 conversion at temperatures below 275 °C, but the CO conversion is higher than the O_2 conversion above 300 °C. The result indicates that the Fe_2O_3 catalyst can be reduced under the reaction mixture above 300 °C. Accordingly, these kinetic measurements were performed at temperatures below 275 °C to avoid the reduction of Fe_2O_3 catalyst during the measurements. In the catalytic CO oxidation, the CO disproportionation ($2CO(g) \rightarrow CO_2(g) + C(s)$) should be considered as a side reaction because the disproportionation can occur below 700 °C from the viewpoint of thermochemistry. According to Li *et al.*,[5] the CO disproportionation on α-Fe_2O_3 nanopowder catalyst occurs above 300 °C in the absence of O_2. In this work, the CO disproportionation as a side reaction is considered to be negligible because these experiments were performed in the presence of O_2 below 275 °C.

The apparent activation energies, obtained in the temperature range of 150-275 °C, are in the range of 13.7-15.0 kcal/mol, as shown in Figure 5. From the magnitude of the apparent activation energies, it is clear that the reactants are chemisorbed on the catalyst surface. Oxygen vacancies in the α-Fe_2O_3 catalyst can be considered as a possible adsorption site for the reactants because they are served as a predominating point defect of the oxide and easily produced by heating the oxide. It is well known that oxygen vacancy defect in metal oxide can act as an electron donor and become an adsorption site for oxygen molecule. O_2(g) can

be adsorbed on oxygen vacancy to be dissociated into two oxygen atoms according to the equilibria: $O_2(g) + 2e^- \rightleftarrows 2O^-(ads)$ and $O^-(ads) + e^- \rightleftarrows O^{2-}(latt)$. It is generally accepted for the Fe_2O_3-catalyzed CO oxidation that $CO_2(g)$ is produced by the interaction between CO(g) and lattice oxygens.[5,15,17] At moderately low temperatures, CO(g) could be adsorbed on lattice oxygen as the following reaction:

$$CO(g) + O^{2-}(latt) \rightleftarrows CO_2^-(ads) + e^- \quad (1)$$

$CO_2^-(ads)$ can further react with $O^-(ads)$ or $O^{2-}(latt)$ to form carbonate ion, which can be represented as the following reactions:

$$CO_2^-(ads) + O^-(ads) \rightleftarrows CO_3^{2-}(ads) \quad (2)$$

$$CO_2^-(ads) + O^{2-}(latt) \rightleftarrows CO_3^{2-}(ads) + e^- \quad (3)$$

$CO_3^{2-}(ads)$ can be decomposed to produce $CO_2(g)$ according to the reaction:

$$CO_3^{2-}(ads) \rightarrow CO_2(g) + O^{2-}(latt) \quad (4)$$

If $CO_2^-(ads)$ reacts with $O^-(ads)$ to form $CO_2(g)$, the partial order with respect to O_2 would be 0.5-order as reported previously.[18] However, the experimental data in Figure 6 show zero-order kinetics for O_2 on both the catalysts, which means that the Fe_2O_3 surface is continuously saturated by oxygen and suggests that the interaction between $CO_2^-(ads)$ and $O^-(ads)$ on the catalysts is not predominant. It has been proposed that the interaction between $CO_2^-(ads)$ and $O^-(ads)$ forms monodentate carbonate, while the interaction between $CO_2^-(ads)$ and $O^{2-}(latt)$ forms bidentate carbonate.[19,20] According to the FT-IR spectroscopy study of CO_2 adsorption on the Fe_2O_3 nanopowder by Baltrusaitis *et al.*,[21] CO_2 is adsorbed on the oxide surface to form bidentate carbonate. Their result supports that the interaction between $CO_2^-(ads)$ and $O^{2-}(latt)$ is favorable on the surface of Fe_2O_3 catalyst.

As shown in Figure 6, the α-Fe_2O_3 fine powder-catalyzed reaction was found to be first-order kinetics for CO. From equilibria (1), (3), and reaction (4), the rate law is as rate $\cong k[CO(g)]$, where $[O^{2-}(latt)]$ and $[e^-]$ are taken to be constant. The rate law is agreeable to the experimental one for the α-Fe_2O_3 fine powder-catalyzed reaction. On the other hand, the partial order with respect to CO for the reaction catalyzed by the Fe_2O_3 spherical submicron clusters was found to be 0.75-order, as shown in Figure 6. The result makes it possible to consider that the reaction obeys a mechanism involving the inhibition process by CO_2. The inhibition process by CO_2 corresponds to the reverse of reaction (4) and can be represented as the following equilibrium:

$$CO_3^{2-}(ads) \rightleftarrows CO_2(g) + O^{2-}(latt) \quad (5)$$

Since CO_2 molecule is more massive than CO and O_2 molecules, the contact time of CO_2 molecule with the inner wall of mesopores of the Fe_2O_3 spherical submicron cluster is expected to be longer than CO and O_2 molecules, which may raise the probability of the interaction between $CO_2(g)$ and $O^{2-}(latt)$ on the inner wall of pores. Reddy *et al.*,[12] have performed a density functional theoretical study on the CO oxidation over Fe_2O_3 clusters and proposed the formation of carbonate complex on the surface of Fe_2O_3 clusters, supporting the possibility of inhibition process by CO_2 in the catalytic processes. The apparent activation energy for the CO consumption on the α-Fe_2O_3 spherical submicron clusters, 13.7 kcal/mol, is somewhat lower than 15.0 kcal/mol obtained on the α-Fe_2O_3 fine powder catalyst. If the rate of CO disappearance on the α-Fe_2O_3 spherical submicron clusters is affected by the CO_2 inhibition, the apparent activation energy would be observed as somewhat lower value than that on the α-Fe_2O_3 fine powder catalyst. Assuming both CO and CO_2 are adsorbed on the same site (lattice oxygen), the rate law can be represented as rate $\cong k(P\text{co}/P\text{co}_2)^\alpha$ ($0 \le \alpha \le 1$), which is similar to that of ammonia decomposition.[22] The 0.75-order with respect to CO, obtained in this work, is agreeable to the rate law with $\alpha = 0.75$.

Consequently, the partial order with respect to CO was found to be first-order on the α-Fe_2O_3 fine powder catalyst, but 0.75-order on the α-Fe_2O_3 spherical submicron powder catalyst. The result indicates that the inhibiting process by CO_2 is involved in the reaction mechanism of the CO oxidation on α-Fe_2O_3 spherical submicron powder. The CO_2 inhibiting effect seems to be closely related to the internal pore structure of the α-Fe_2O_3 spherical submicron clusters. A diffusion limitation of gaseous reactants into the pores may cause the observation of lower rate. Namely, when the number of molecules introducing into the internal mesopores is limited, the number of molecules reacting on the inner wall of pore would be smaller than those on the outer surface of catalyst, which results in the observation of different kinetics between the α-Fe_2O_3 spherical submicron clusters- and the α-Fe_2O_3 fine powder-catalyzed reactions. Although the diffusion effect cannot be entirely excluded in this work, the observation of lower partial order of CO on the α-Fe_2O_3 spherical submicron clusters is believed to be due to the interaction between product CO_2 and lattice oxygens on the inner surface of pore. It is suggested from the kinetic results that the spherical submicron clusters of α-Fe_2O_3 nanoparticles are utilizable as an adsorbent material for CO_2 capture.

Acknowledgments. This work was supported by a grant from the Converging Research Center Program through the Ministry of Science, ICT and Future Planning, Korea (2013K000426). S.-H. Lee thanks a grant from the basic Science and Research Program of the KOSEF (No. 2009-0077906).

References

1. Haruta, M.; Tsubota, S.; Kobayashi, T.; Kageyama, H.; Genet, M. J.; Delmon, B. *J. Catal.* **1993**, *144*, 175.
2. Kahlich, M. J.; Gasteiger, H. A.; Behm, R. J. *J. Catal.* **1999**, *182*, 430.
3. Oran, U.; Uner, D. *Appl. Catal. B* **2004**, *54*, 183.
4. Liu, L.; Zhou, F.; Wang, L.; Qi, X.; Shi, F.; Deng, Y. *J. Catal.* **2010**, *274*, 1.
5. Li, P.; Miser, D. E.; Rabiei, S.; Yadav, R. T.; Hajaligol, M. R. *Appl.*

Catal. B **2003**, *43*, 151.
6. Ma, X. H.; Feng, X. Y.; Song, C.; Zou, B. K.; Ding, C. X.; Yu, Y.; Chen, C. H. *Electrochem. Acta* **2013**, *93*, 131.
7. Guo, Z. P.; Yuan, L.; Konstantinov, K.; Huang, Z. G.; Liu, H. K. *Mat. Lett.* **2006**, *60*, 3891.
8. Yin, S.; Xue, W.; Ding, X. L.; Wang, W. G.; He, S. G.; Ge, M. F. *Int. J. Mass Spec.* **2009**, *281*, 72.
9. Oh, H. D.; Lee, S. W.; Kim, S. O.; Lee, J. K. *J. Power Source* **2013**, *244*, 575.
10. Reilly, N. M.; Reveles, J. U.; Johnson, G. E.; del Campo, J. M.; Khanna, S. N.; Castleman, A. W., Jr. *J. Phys. Chem. C* **2007**, *111*, 19086.
11. Broclawik, E.; Haber, J.; Piskorz, W. *Chem. Phys. Lett.* **2001**, *333*, 332.
12. Reddy, B. V.; Rasouli, F.; Hajaligol, M. R.; Khanna, S. N. *Fuel* **2004**, *83*, 1537.
13. Deng, H.; Li, X.; Peng, Q.; Wang, X.; Chen, J.; Li, Y. *Angew. Chem. Int. Ed.* **2005**, *44*, 2782.
14. Reymond, J. P.; Meriaudeau, P.; Teichner, S. J. *J. Catal.* **1982**, *75*, 39.
15. Kaneko, K. *J. Memb. Sci.* **1994**, *96*, 59.
16. Cao, J. L.; Wang, Y.; Yu, X. L.; Wang, S. R.; Wu, S. H.; Yuan, Z. Y. *Appl. Catal. B* **2008**, *79*, 16.
17. Oliveira, L. C. A.; Fabris, J. D.; Rios, R. R. V. A.; Mussel, W. N.; Lago, R. M. *Appl. Catal. A* **2004**, *259*, 253.
18. Jung, H. J.; Lim, J. T.; Lee, S. H.; Kim, Y. R.; Choi, J. G. *J. Phys. Chem.* **1996**, *100*, 10243.
19. Hertl, W. *J. Catal.* **1973**, *31*, 231.
20. Yanagisawa, Y.; Takaoka, K.; Yamake, S.; Ito, T. *J. Phys. Chem.* **1995**, *99*, 3704.
21. Baltrusaitis, J.; Schuttlefield, J.; Zeitler, E.; Grassian, V. H. *Chem. Eng. J.* **2011**, *170*, 472.
22. Anderson, J. R., Boudart, M., Eds., *Catalysis Science and Technology Vol.1*; Springer-Verlag: New York, 1981; p 115.